

# Synthesis of Cyclen-Functionalized Ethenylene-Based Periodic Mesoporous Organosilica Nanoparticles and Metal-Ion Adsorption Studies

Hao Li,<sup>[a, b]</sup> Ani Vardanyan,<sup>[c]</sup> Clarence Charnay,<sup>[b]</sup> Laurence Raehm,<sup>[b]</sup>  
Gulaim A. Seisenbaeva,<sup>\*,[c]</sup> Roser Pleixats,<sup>\*,[a]</sup> and Jean-Olivier Durand<sup>\*,[b]</sup>

**Abstract:** The preparation of two cyclens both possessing two triethoxysilyl groups through click chemistry is described. These two cyclens were incorporated into bis(triethoxysilyl) ethenylene-based periodic mesoporous organosilica nanoparticles (PMO NPs) at different proportions of bis(triethoxysilyl)ethenylene/cyclens (90/10, 75/25). The obtained nanorods were analyzed with different techniques and showed high specific surface areas at low proportion of

cyclens. The nanorods containing free amino groups of cyclen were then used for Ni(II) and Co(II) removal from model solutions. The kinetics and isotherms of adsorption of Ni(II) and Co(II) were determined, and the materials showed high uptake of metals (up to 3.9 mmol·g<sup>-1</sup>). They demonstrated pronounced selectivity in separation of rare earth elements from late transition metals, e.g. Ni(II) and Co(II) by adsorption and even more so by controlled desorption.

## 1. Introduction

The development of Mesoporous Organosilica Nanoparticles (MON) has grown a lot the last decade for different applications, mainly drug delivery, but also catalysis. The field has been comprehensively reviewed<sup>[1]</sup> and recent examples have shown elaboration of complex core-shell structures allowing sequential release of hydrophobic and hydrophilic drugs.<sup>[2]</sup> Regarding the emerging environmental applications field, the extraction of heavy metal ions from water was studied. Hybrid organic-inorganic mesoporous silica-based materials in bulk were first investigated. For instance, carbon dots-modified mesoporous organosilica,<sup>[3]</sup> amino and thiol functionalized phenylene-bridged Periodic Mesoporous Organosilicas (PMO),<sup>[4]</sup> or SBA-15 based mesoporous silica hybrid adsorbents<sup>[5]</sup> were reported. The topic has been comprehensively reviewed as well.<sup>[6]</sup> Recently, the use of nanoparticles instead of bulk materials allowed to increase the outer specific surface area of the materials. Yang et al, prepared ferrocene-based MON for the

extraction of phosphates and Pb(II).<sup>[7]</sup> Kaczmarek et al. synthesized amine-modified bis(triethoxysilyl)ethane-based PMO NPs which acted as sensors for Hg(II) and other metal ions after functionalization with Schiff bases.<sup>[8]</sup> A sophisticated bis(triethoxysilyl)ethane and Fe<sub>3</sub>O<sub>4</sub>-based Janus nanocube was synthesized by Su et al. for the removal of Au(III).<sup>[9]</sup> As aza macrocycles such as cyclens are very efficient metal ion chelators,<sup>[10]</sup> we thought of preparing cyclen-based PMO NPs for heavy metal water removal. We present here the synthesis of BOC-protected bis(triethoxysilyl)-functionalized cyclen precursors through click reaction and their incorporation in PMO NPs with bis(triethoxysilyl)ethenylene (E). After characterization of the materials and cleavage of BOC protecting groups, Ni(II) and Co(II) removal from model solutions and their separation from Rare Earth Elements (REE) was studied.

## 2. Results and Discussion

### 2.1. Preparation and characterization of silylated precursors and nanomaterials

Two bis-silylated cyclen derivatives **P1** and **P2** were envisaged as precursors for the preparation of periodic mesoporous organosilica nanoparticles (PMO NPs).

Alkyne **3** was obtained in two steps from commercial cyclen **1** through the *tri*-BOC intermediate **2** following procedures described in the literature (Scheme 1).<sup>[11]</sup> A copper-catalyzed alkyne azide cycloaddition reaction (CuAAC)<sup>[12]</sup> of the alkyne **3** with the corresponding bis(silylated azide), using the system Cu(I)/TBTA in a mixture of Et<sub>3</sub>N/THF at 50 °C under anhydrous conditions, provided the disilylated precursors **P1** and **P2** in 93% and 88% isolated yields, respectively. Note that Cu(II) was not complexed by cyclen as BOC groups were present. Compounds **P1** and **P2** were fully characterized by <sup>1</sup>H and <sup>13</sup>C NMR spectroscopy (Figure S1). The complete characterization of

[a] H. Li, Prof. R. Pleixats

Department of Chemistry and Centro de Innovación en Química Avanzada (ORFEO-CINQA), Universitat Autònoma de Barcelona, 08193-Cerdanyola del Vallès, Barcelona (Spain)  
E-mail: roser.pleixats@uab.cat

[b] H. Li, Dr. C. Charnay, Dr. L. Raehm, Dr. J.-O. Durand

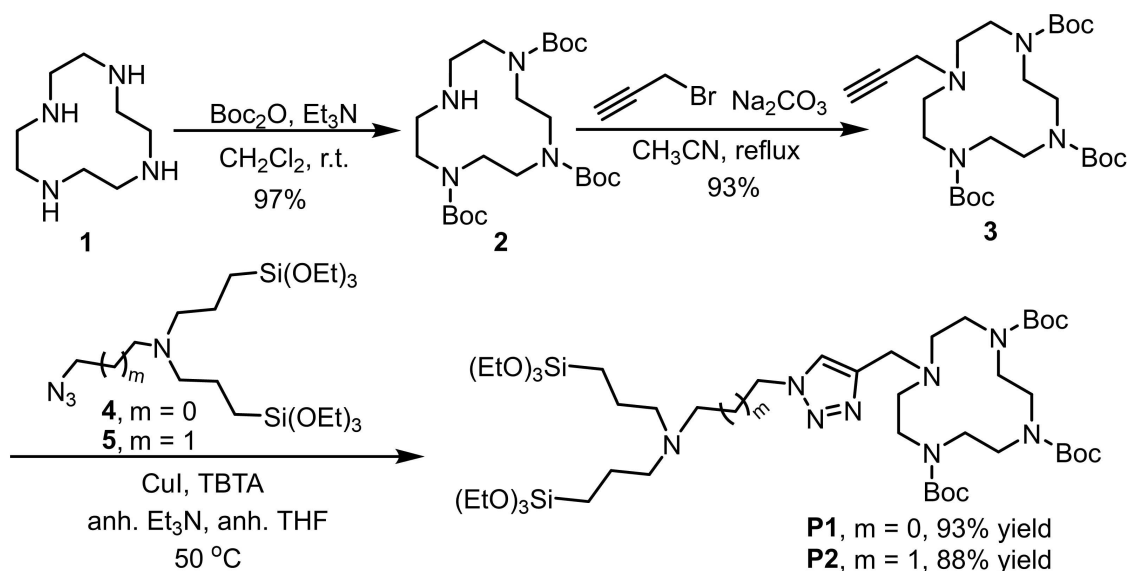
ICGM, Univ. Montpellier, CNRS, ENSCM, Case 1701, Place Eugène Bataillon, CEDEX 05, 34095 Montpellier (France)  
E-mail: jean-olivier.durand@umontpellier.fr

[c] Dr. A. Vardanyan, Prof. G. A. Seisenbaeva

Department of Molecular Sciences, Swedish University of Agricultural Sciences, 750 07 Uppsala (Sweden)  
E-mail: gulaim.seisenbaeva@slu.se

Supporting information for this article is available on the WWW under <https://doi.org/10.1002/cnma.202000383>

© 2020 The Authors. Published by Wiley-VCH GmbH. This is an open access article under the terms of the Creative Commons Attribution License, which permits use, distribution and reproduction in any medium, provided the original work is properly cited.



Scheme 1. Synthesis of precursors P1 and P2.

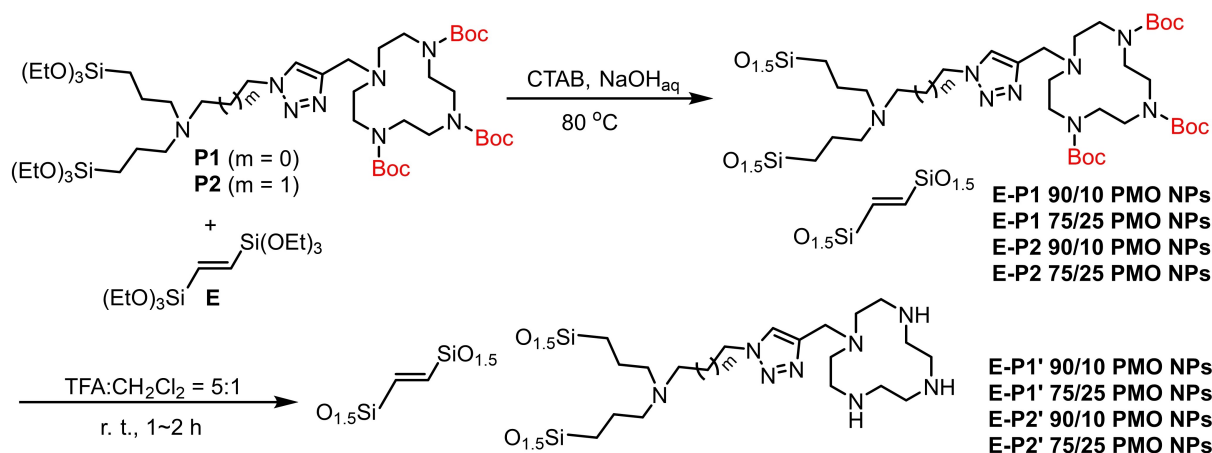
the molecules was achieved by 1D and 2D NMR experiments (1D  $^1\text{H}$ , 2D  $^1\text{H}$ - $^1\text{H}$  COSY, TOCSY and NOESY, 2D  $^1\text{H}$ - $^{13}\text{C}$  HSQC and HMBC) and the coordinated analysis of the resulting spectra (see details in the Supporting Information, Figure S2 and Table S1).

With those precursors P1 and P2 in hand, four PMO NPs were prepared. We mixed disilylated precursors E and P1 (leading to E-P1 PMO NPs) at a proportion of E/P1 of 90/10 or 75/25. Mixing E and P2 lead to E-P2 PMO NPs, at a proportion E/P2 of 90/10 or 75/25 (Scheme 2). The syntheses were performed in Milli-Q water with CTAB as template under basic catalysis (NaOH). The micellar solution was prepared at 80 °C for 50 min with a stirring speed adjusted at 1000 rpm. Then, the stirring speed was enhanced to 1400 rpm. A mixture of (E) and different amounts of the corresponding disilylated precursor Pn was quickly added and the mixture was left to react for 120 mins at 80 °C.<sup>[13]</sup> E-P1 90/10 PMO NPs, E-P1 75/25 PMO NPs, E-

P2 90/10 PMO NPs and E-P2 75/25 PMO NPs were collected by centrifugation, the template was removed by washing with a solution of  $\text{NH}_4\text{NO}_3$  (6 g/L in 96% EtOH).

BOC groups were then cleaved by treatment with TFA to lead to E-P1' 90/10 PMO NPs, E-P1' 75/25 PMO NPs, E-P2' 90/10 PMO NPs and E-P2' 75/25 PMO NPs. The cleavage of the BOC group was assessed by solid-state  $^{13}\text{C}$  MAS NMR with the disappearance of the signals at 156 ppm (C=O), 80 ppm ( $\text{C}_q$ ), 29 ppm (Me groups) (see the Supporting Information, Figure S3 and Figure S4). FTIR also confirmed the cleavage of BOC with the disappearance of the band at  $1670\text{ cm}^{-1}$  ( $\gamma$  C=O) (Figure S5).

The materials were analyzed with different techniques. Transmission Electron Microscopy (TEM) (Figure 1 and Figure S6) showed that nanorods were obtained (500–700 nm length, 100 nm width) with a wormlike porosity. Small angle XRD (Figure S7) confirmed the low organisation of the porosity.



Scheme 2. Preparation of E-P1 PMO NPs, E-P1' PMO NPs, E-P2 PMO NPs and E-P2' PMO NPs (proportion 90/10 and 75/25).

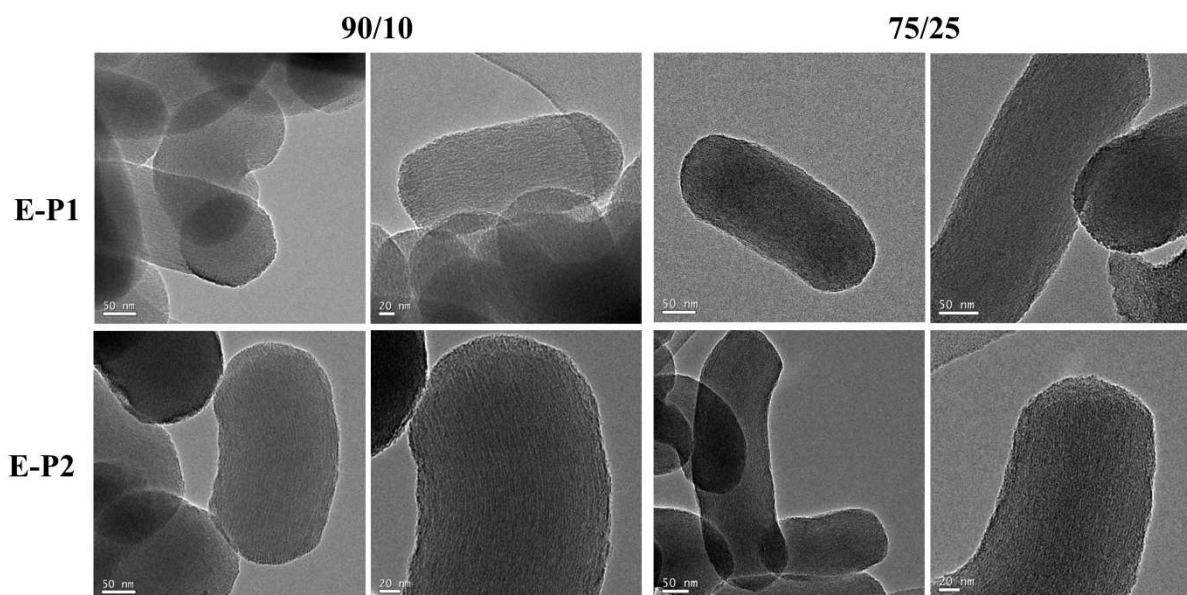


Figure 1. TEM images of E-P1 90/10, E-P1 75/25, E-P2 90/10 and E-P2 75/25 PMO NPs, at two different magnifications (scale bar 50 and 20 nm).

The textural characteristics of E-Pn' PMO NPs were investigated by Atomic Force Microscopy (AFM) (Figure 2). The samples were deposited as dry powder onto a doubly gluing carbon tape. Aggregated periodic mesoporous organosilica nanoparticles were clearly distinguishable on AFM images. The AFM data of E-Pn' PMO NPs was in agreement with TEM

analysis of E-Pn PMO NPs. The surface of the particles is apparently rough with shapes, indicating regular pore openings.

Data for N<sub>2</sub> sorption experiments, dynamic light scattering (DLS), zeta potential, thermogravimetric analyses (TGA) are reported in Table 1.

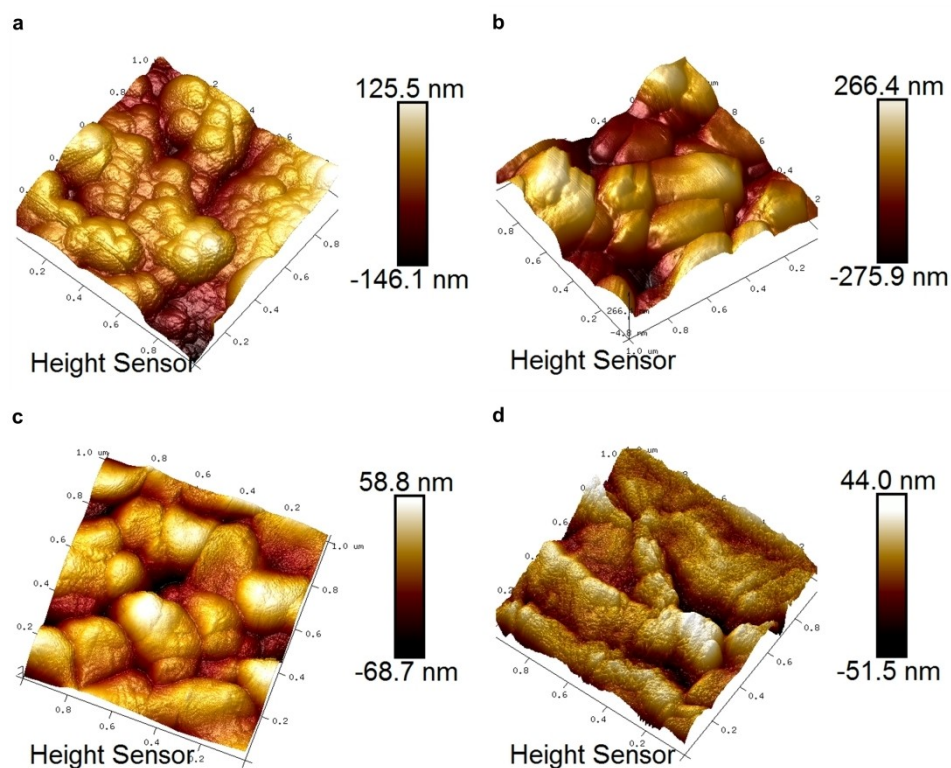


Figure 2. AFM images of E-P1' 90/10 PMO NPs (a); E-P1' 75/25 PMO NPs (b); E-P2' 90/10 PMO NPs (c) and E-P2' 75/25 PMO NPs (d).

**Table 1.** Data for E-P1 PMO NPs, E-P1' PMO NPs, E-P2 PMO NPs and E-P2' PMO NPs.

PMO NPs	N <sub>2</sub> -sorption measurements		DLS [nm]	Zeta potential		TGA <sup>c</sup> [%]	
	S <sub>BET</sub> m <sup>2</sup> ·g <sup>-1</sup>	V <sub>pore</sub> cm <sup>3</sup> ·g <sup>-1</sup> <sup>a</sup>		∅ <sub>pore</sub> nm <sup>b</sup>	pH		mV
E-P1 90/10 PMO NPs	513	0.29	2.3	520	6.66	39.4	60
E-P2 90/10 PMO NPs	492	0.25	2.0	621	6.25	34.0	68
E-P1 75/25 PMO NPs	162	0.09	2.2	639	6.08	32.7	53
E-P2 75/25 PMO NPs	nd <sup>d</sup>	nd	nd	463	4.66	41.2	55
E-P1' 90/10 PMO NPs	705	0.43	2.4	nd	5.30	42.5	nd
E-P2' 90/10 PMO NPs	645	0.34	2.1	nd	5.34	40.3	nd
E-P1' 75/25 PMO NPs	202	0.10	2.1	nd	5.31	38.6	nd
E-P2' 75/25 PMO NPs	nd	nd	nd	nd	5.30	39.6	nd

<sup>a</sup>) Determined by BET at saturation of p/p<sup>0</sup> = 0.8; <sup>b</sup>) Pore diameter determined with BJH; <sup>c</sup>) Residual mass by TGA (heating rate 10 °C/min, 20 to 1000 °C); <sup>d</sup>) Not determined.

DLS data agreed with TEM images showing hydrodynamic diameters ranging from 463 nm to 639 nm (Figure S8). Positive zeta potentials were observed in agreement with the protonation of the amine groups constituting the materials (Figure S9). TGA analyses showed the loss of water from 0 to 100 °C then decomposition of BOC group occurred from 150 to 250 °C, and finally the loss of the remaining organic part was observed from 300 to 800 °C (Figure S10).

Brunauer-Emmett-Teller (BET) technique was used to monitor the porosity and specific surface area of the PMO NPs (Table 1). Materials E-P1 90/10 PMO NPs and E-P1' 90/10 PMO NPs (Figure 3) showed type IV isotherms with a narrow hysteresis at 0.3 P/P<sup>0</sup> characteristic of mesoporous materials with small pore sizes of 2.3 nm (from BJH method). The specific surface area increased by removing the BOC group from 513 to

705 m<sup>2</sup>·g<sup>-1</sup> in agreement with a better accessibility of the porosity. E-P2 90/10 PMO NPs and E-P2' 90/10 PMO NPs materials showed between type II and type IV isotherms characteristic of an important microporous contribution to the porosity. The small pore size was 2 nm. The same trend was observed as before with an increase of the specific surface area upon removal of the BOC group.

By increasing the proportion of cyclens in the materials, the specific surface area and porosity volume dropped (E-P1 75/25 PMO NPs 162 m<sup>2</sup>·g<sup>-1</sup>, E-P1' 75/25 PMO NPs 202 m<sup>2</sup>·g<sup>-1</sup>).

The content of cyclen moiety in the nanomaterials E-Pn' was estimated from the content of nitrogen from EDS analysis (Table 2 and Table S2). For example, the cyclen loading of E-P1' 90/10 PMO NPs was 0.56 mmol·g<sup>-1</sup>. In Figure 4 we gather the SEM image and the corresponding element mapping of E-P1'

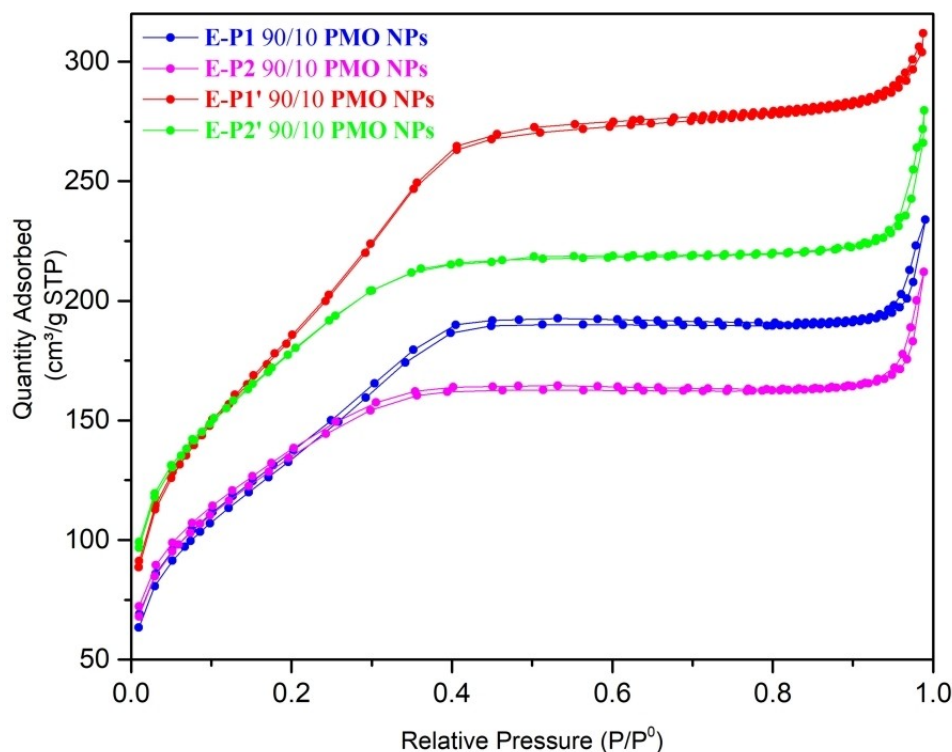


**Figure 3.** BET isotherms of E-P1 90/10 PMO NPs, E-P2 90/10 PMO NPs, E-P1' 90/10 PMO NPs and E-P2' 90/10 PMO NPs.

PMO NPs	Si [%]	C [%]	O [%]	N [%]	Cyclen loading [mmol/g] <sup>[b]</sup>
E-P1' 90/10 PMO NPs	32.67	28.27	32.81	6.26	0.56
E-P1' 75/25 PMO NPs	28.08	27.46	33.58	8.33	0.74
E-P2' 90/10 PMO NPs	28.70	32.43	35.09	3.78	0.34
E-P2' 75/25 PMO NPs	23.62	38.15	30.29	7.95	0.71

<sup>[a]</sup> Each sample was investigated on three different areas and the average value was taken; <sup>[b]</sup> Calculated from the N elemental analysis of EDS.

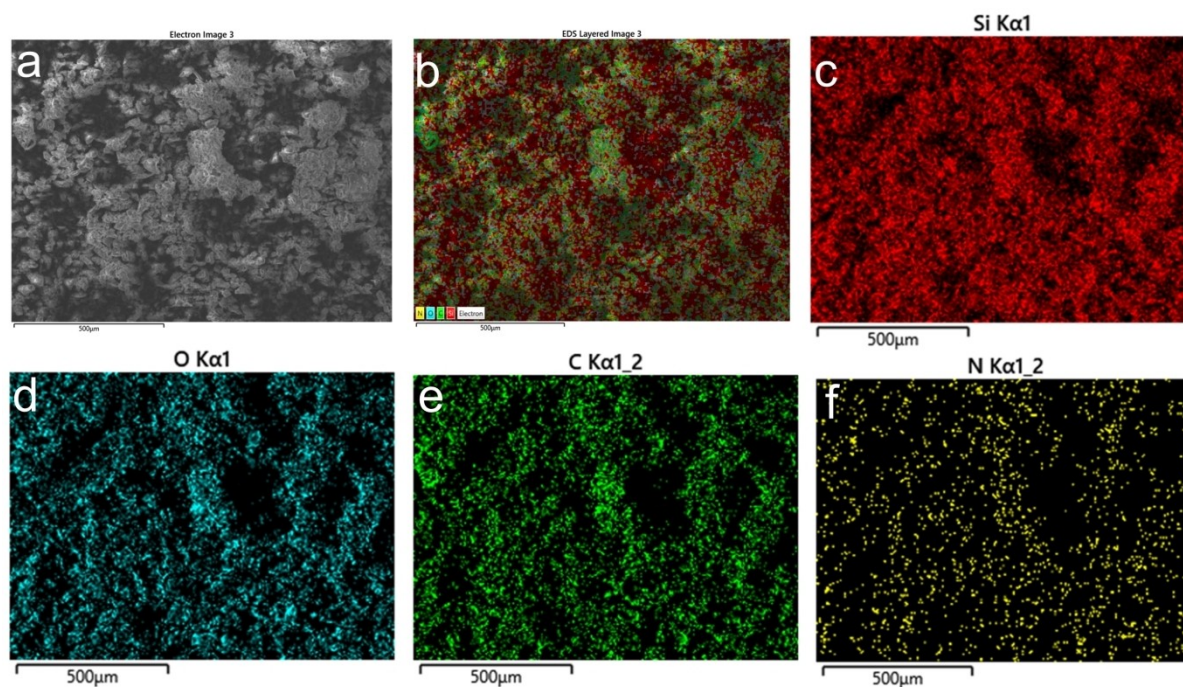


Figure 4. SEM image of E-P1' 90/10 PMO NPs (a); corresponding element mapping: all the elements (b), Si (c), O (d), C (e) and N (f).

90/10 PMO NPs. Element distribution is rather even following the apparent morphology of the particles. The peaks corresponding to nitrogen clearly indicate the presence of cyclen moiety in the nanoparticles (see the element mapping for E-P1' 75/25, E-P2' 90/10 and E-P2' 75/25 PMO NPs in Figures S11–S13 in the supporting information).

## 2.2. Adsorption studies of Ni(II) and Co(II)

The adsorption of Ni(II) and Co(II) from water by E-Pn' PMO NPs was assayed. At first, the adsorption kinetics for E-P1' 90/10 PMO NPs was determined (Figure 5 and Table S3).

Adsorption kinetics showed that most of the uptake (80%) occurs during the first hour of interaction of metals with E-P1' 90/10 PMO NPs. Slower adsorption continues and equilibrium is reached after 20 hours. The same trend was observed for the other three samples: E-P1' 75/25, E-P2' 90/10 and E-P2' 75/25 PMO NPs (Figure S14). Next, the adsorption isotherms were carried out with the E-P1' 75/25, E-P2' 90/10 and E-P2' 75/25 PMO NPs samples. Broad range of concentrations of heavy

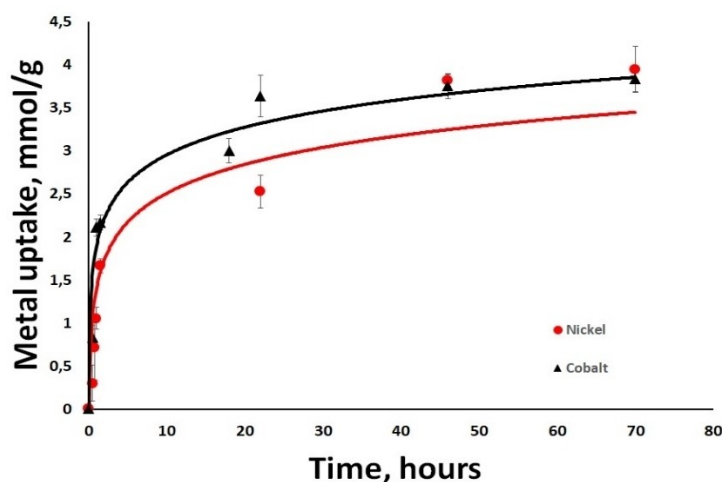


Figure 5. Adsorption kinetics of E-P1' 90/10 PMO NPs for Ni(II) and Co(II).

metals was chosen for these experiments (0.5 mM, 1 mM, 5 mM, 10 mM, 20 mM and 25 mM) (Figure 6).

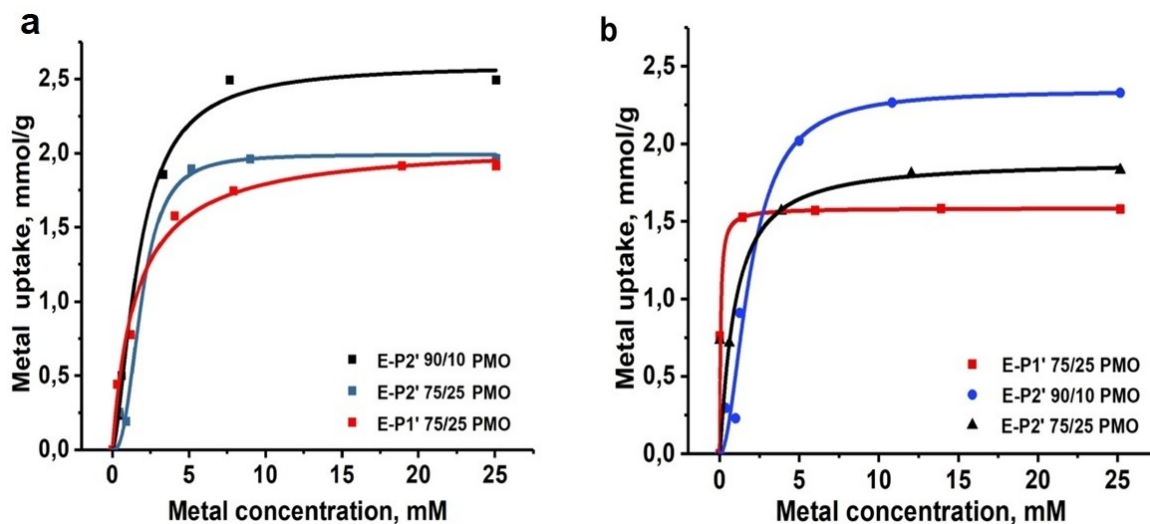


Figure 6. Adsorption isotherms of E-P1' 75/25 PMO NPs, E-P2' 90/10, E-P2' 75/25 PMO NPs for (a) Ni(II) and (b) Co(II).

All the uptake isotherms fitted well with Langmuir curves, having high R square values (between 0.98–0.99). The saturation occurred at 5 mM or even below for E-P1' 75/25 PMO NPs. Table 3 shows the average maximum adsorption capacity for each nanoadsorbent and heavy metal cation ( $\text{Ni}^{2+}$  and  $\text{Co}^{2+}$ ).

E-P1' 90/10 PMO NPs showed the highest metal uptake (Figure S14) in agreement with its highest specific surface area and pore size. It appears that the adsorption capacity results from combined contribution from both the surface area and the ligand content. Indeed if only specific surface area ( $S_{\text{BET}}$ ) or Cyclen Loading is considered, metal adsorption capacity do not show any clear correlation (Figure S15).

When set as a combined parameter, the content of Cyclen ligand and the surface area reveal linear correlation with the quantity of adsorbed cations (Table S4, Figure S16 and Figure 7).

When the ratio of E and Pn is 90/10, the observed ratio of Cyclen Ligand/Metal is approximately 1:7, while when the ratio of E and Pn is 75/25, the observed Cyclen Ligand/Metal ratio is 1:2–3. This indicates that the uptake is strongly driven by the interactions of metal cations with the external and internal surface of hybrid particles, possibly even in the form of surface silicates. Formation of the latter may be favored by local basic conditions in the pores induced by the presence of Cyclen ligands. It seems that chelation within a Cyclen ring is also contributing to the mechanism of uptake. This indicates a

considerable difference for the uptake in mesoporous nanoparticles compared to that of dense nanoparticles, where coordination of metal cations most often can be related to complexation in the monolayer on the surface.<sup>[14]</sup> The mapping of Ni(II) on E-P1' 75/25 PMO NPs and its quantification (Table S5 and Table S7) was performed with EDS (Figures S17–S18) after adsorption of an aqueous solution of Ni(II) at 0.5 and 10 mM initial metal concentration, respectively. We observed a homogeneous distribution of Ni(II) in the nanorods with an adsorption of  $0.46 \text{ mmol}\cdot\text{g}^{-1}$  and  $0.94 \text{ mmol}\cdot\text{g}^{-1}$  of Ni(II), respectively.

Desorption tests for E-P2' 90/10 PMO NPs and E-P1' 75/25 PMO NPs were performed with 1 M nitric acid (Table 4). The desorption rates were analyzed by titration of the metal with EDTA for Co(II) and Ni(II). EDS analysis with E-P1' 75/25 PMO NPs was also performed for the remaining Ni(II) after desorption (Table S6 and Table S8).

We obtained 80% of Ni(II) desorption based on EDS (Tables S5–S8), but only 59% for Co(II), with E-P1' 75/25 PMO NPs. In the case of E-P2' 90/10 PMO NPs, the desorption values for Ni(II) and Co(II) were 79% and 42%, respectively. Co(II) was therefore more strongly adsorbed than Ni(II).

Selective adsorption and desorption of organosilica nanoparticles (E-P2' 75/25 PMO NPs) were tested with two different metal mixtures, namely cobalt-samarium and nickel-neodymium which are relevant for recycling of components for the REE-based magnets. For this procedure, after the first adsorption/desorption cycle, 10 mg nanoparticles were mixed with equimolar metal mixtures of Nd–Ni and Co–Sm (5 mM initial

Table 3. Average maximum adsorption capacity for each nanoadsorbent and heavy metal (mmol/g).

Sample	Ni	Co
E-P1' 90/10 PMO NPs	3.94	3.84
E-P1' 75/25 PMO NPs	1.91	1.58
E-P2' 90/10 PMO NPs	2.49	2.33
E-P2' 75/25 PMO NPs	1.96	1.83

Table 4. Nickel and Cobalt desorption rates for two organosilica nanoparticle samples.

Metal	E-P1' 75/25 PMO NPs	E-P2' 90/10 PMO NPs
Nickel(II)	80%	79%
Cobalt(II)	59%	42%

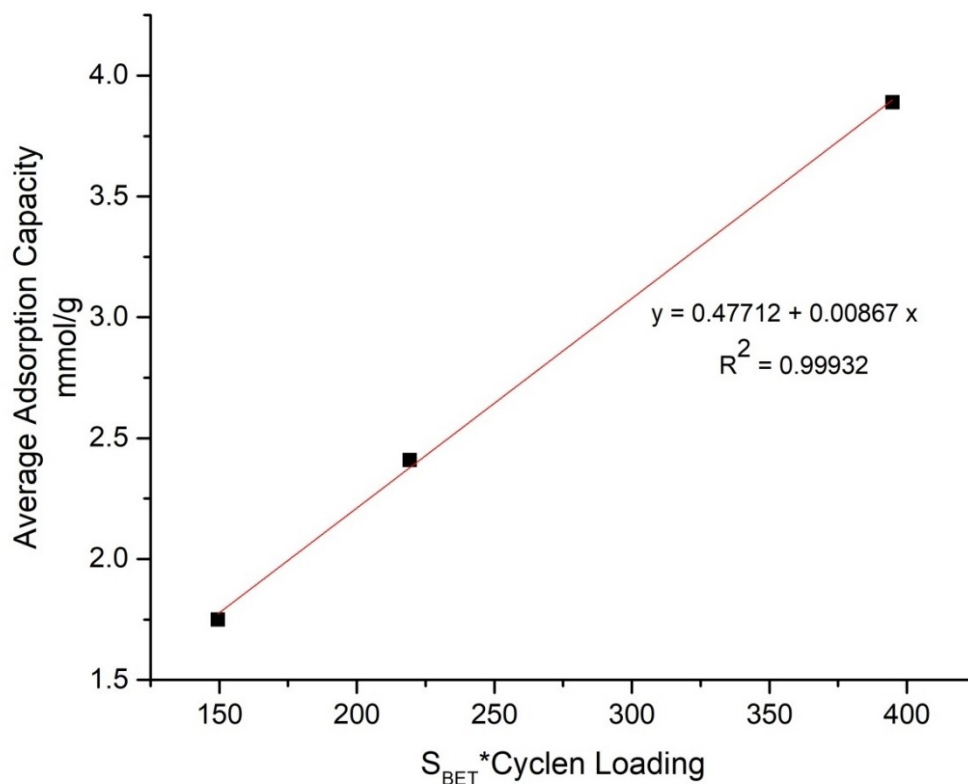


Figure 7. Average adsorption capacity of metals (II) as function of  $S_{\text{BET}} \cdot \text{Cyclen Loading}$ .

concentration each) for 24 hours. Subsequently, nanoparticles were separated by centrifugation (7000 rpm), dried under nitrogen atmosphere and the metal content on the surface was analyzed by EDS. Results showed higher selectivity towards Ni ions, with a Ni/Nd ratio of approximately 5.5:1 (Figure S19 and Table S9). Lower selectivity was observed for cobalt ions and the ratio of Co/Sm was 1.75:1 (Figure S20 and Table S10). Selective desorption was carried out with nitric acid at pH=3.5 in 50 mL falcon tubes. 10 mg nanoparticles were mixed with 10 mL acid solutions and shaken for 24 hours. Subsequently, the nanoparticles were separated by centrifugation (7000 rpm) and dried under nitrogen atmosphere. EDS analysis showed good selectivity towards Co and Ni with high Ni/Nd=7:1 and Co/Sm=8.5:1 ratios (Tables S11 and Table S12). Therefore desorption was selective for REE. This indicates that the ligand contribution was important and these mesoporous nanoadsorbents could be used in separation of REE from heavy transition metals.

### 3. Conclusion

In summary, we have synthesized two disilylated cyclen based derivatives **P1** and **P2** containing Boc groups through a copper-catalyzed azide-alkyne cycloaddition (CuAAC). Mixed periodic mesoporous organosilica nanoparticles (PMO NPs) were prepared from these precursors **Pn** and bis(triethoxysilyl)ethylenylene, **E**, at different proportions of **E/Pn** (90/10, 75/25). The Boc

groups of **E-Pn PMO NPs** were removed by treatment with trifluoroacetic acid to afford **E-Pn'** PMO NPs containing cyclen moieties with coordinating amino groups. The obtained nanorods were analyzed with different techniques (TEM, AFM,  $\text{N}_2$ -sorption measurements, DLS, zeta potential, TGA, EDS), and showed high specific surface areas at low proportion of **Pn**. The **E-Pn'** PMO NPs nanorods were then used for efficient removal of Ni(II) and Co(II) from aqueous solutions. The kinetics and isotherms of adsorption of Ni(II) and Co(II) were determined, and the nanomaterials showed high uptake of metals of up to 3.9 and 3.8  $\text{mmol} \cdot \text{g}^{-1}$  for nickel and cobalt, respectively. The uptake mechanism is complex, indicating the combined role of the active surface area of mesoporous silica and its pore volume along with the ligand content. The obtained hybrid nano-adsorbents revealed considerable selectivity in separation of REE from late transition metals, especially on controlled desorption. This may be due to the generally accepted difference in adsorption mechanisms based on inner sphere coordination complexation for Ni(II) and Co(II), and outer sphere mostly electrostatic binding for REE.<sup>[15]</sup>

### Experimental Section

**General information.** The  $^{13}\text{C}$  CP-MAS solid state NMR spectra, the surface areas, dynamic light scattering (DLS) and Zeta potential were obtained from University of Montpellier.  $^{13}\text{C}$  CP-MAS NMR spectra were recorded with a Varian V NMRS 300 MHz instrument (Les Ullis, France). The surface areas were determined by the

Brunauer-Emmett-Teller (BET) method from N<sub>2</sub> adsorption-desorption isotherms. The samples were measured with a Micromeritics ASAP2020 analyzer (Mérignac, France) after degassing for 12 h at 80 °C under vacuum. The total pore volumes were evaluated by converting the volume adsorbed at p/p° 0.8 to the volume of liquid adsorbed (single point adsorption total pore volume of pores less than 4000 Å at p/p° ≈ 0.98). The pore size distributions for PMO NPs were determined from the desorption branch using the Barrett-Joyner-Halenda (BJH) method, which relies on the Kelvin equation to relate the width of the pores to the condensation pressure. DLS analyses were performed using a Cordouan Technologies DL 135 (Pessac, France) particle size analyzer instrument. Zeta potential measurements were performed on MALVERN Instruments ZETA SIZER Nano series (Orsay, France) with 1–3 mg samples dispersed in 5 mL of distilled water. The <sup>1</sup>H and <sup>13</sup>C NMR spectra were obtained from *Servei de Resonància Magnètica Nuclear* of the *Universitat Autònoma de Barcelona* (UAB) with Bruker DPX-360 MHz (Bruker Biospin, Rheinstetten, Germany). Mass-spectrometry (MS), elemental analysis and infra-red spectra (IR) were recorded from the *Servei d'Anàlisi Química* of the UAB. Powder X-ray diffraction (P-XRD) was performed with X'Pert Power (PANalytical, Almelo, Netherlands), 45Kv/40 mA, K<sub>α</sub> 1.5419 Å with a cooper anode from the *Servei de Difracció de Raigs X* of UAB. Transmission Electron Microscopy (TEM) was performed on JEM-2011 Electron Microscope 200 Kv (JEOL Ltd., Akishima, Tokyo, Japan), which belongs to the *Servei de Microscòpia* of UAB. Surface structures of samples were studied using a Bruker FastScan Bio Atomic Force Microscope (AFM) in ScanAsyst mode. The FastScan B cantilevers with extremely sharp tip size of 5 nm were used to achieve high resolution. The estimation of the amounts of the elements was carried out by a SEM-EDS technique using a Flex-SEM 1000 II scanning electron microscope. These two equipments belong to the Swedish University of Agricultural Sciences. If necessary, experiments were carried out in Schlenk techniques with standard high vacuum. CTAB, NH<sub>4</sub>NO<sub>3</sub>, sodium hydroxide, potassium bromide and some reagents were purchased from Sigma-Aldrich. Ethanol and acetone was purchased from Fisher Chemicals and hydrochloric acid from VWR PROLABO.

**Synthesis of tri-tert-butyl 10-((1-(2-(bis(3-(triethoxysilyl)propyl)amino ethyl)-1H-1,2,3-triazol-4-yl)methyl)-1,4,7,10-tetraazacyclododecane-1,4,7-tricarboxylate, P1:** To a dry, 100 mL Schlenk flask equipped with a stir bar and under Argon atmosphere, CuI (7.60 mg, 0.04 mmol), TBTA (21.20 mg, 0.04 mmol) and anhydrous THF (20 mL) were added. The resulting mixture was stirred for 30 min, then tri-tert-butyl 10-(prop-2-yn-1-yl)-1,4,7,10-tetraazacyclododecane-1,4,7-tricarboxylate **3** (1.02 g, 2.0 mmol), N-(2-azidoethyl)-3-(triethoxysilyl)-N-(3-(triethoxysilyl)propyl)propan-1-amine **4** (0.99 g, 2.0 mmol) and anhydrous Et<sub>3</sub>N (1.0 mL, 0.73 g/mL 7.2 mmol) were added by using a syringe. The resulting mixture was stirred at 50 °C (Argon atmosphere) until **3** was fully consumed (48 h, TLC monitoring). Then, the solvent was evaporated under reduced pressure and anhydrous hot pentane was added to the residue to extract the bis-silylated product, this digestion with hot pentane was repeated several times and the pentane extracts were concentrated under reduced pressure to provide the pure product **P1** as colorless oil (1.87 g, 93% yield). <sup>1</sup>H NMR (360 MHz, CDCl<sub>3</sub>) δ (ppm): 7.50 (s, 1H), 4.35 (t, J = 7.2 Hz, 2H), 3.89 (s, 2H), 3.81 (q, J = 7.2 Hz, 12H), 3.56 (br s, 4H), 3.36 (br s, 8H), 2.88 (t, J = 7.2 Hz, 2H), 2.69–2.62 (m, 4H), 2.46 (t, J = 7.2 Hz, 4H), 1.46–1.43 (m, 27 + 4H), 1.21 (t, J = 7.2 Hz, 18H), 0.54 (t, J = 7.2 Hz, 4H); <sup>13</sup>C NMR (151 MHz, CDCl<sub>3</sub>) δ (ppm): 156.3, 155.9, 155.5, 141.6, 123.8, 79.7, 79.5, 79.3, 58.5, 57.2, 54.4, 53.2, 50.2, 49.0, 47.8, 45.3, 28.9, 28.7, 28.6, 20.5, 18.5, 8.0. IR (film): 2972.7, 2927.5, 2883.9, 2811.6, 2097.6, 1685.9, 1458.1, 1412.6, 1364.2, 1248.7, 1157.1, 1074.7, 953.3, 771.2 cm<sup>-1</sup>. MS (ESI) m/z: 1005.6 [M + H]<sup>+</sup>, 713.4, 595.4, 403.3; HRMS (ESI) m/z [M + Na]<sup>+</sup> calcd for C<sub>46</sub>H<sub>92</sub>N<sub>8</sub>O<sub>12</sub>Si<sub>2</sub>: 1027.6265, found: 1027.6233.

**Synthesis of tri-tert-butyl 10-((1-(3-(bis(3-(triethoxysilyl)propyl)amino propyl)-1H-1,2,3-triazol-4-yl)methyl)-1,4,7,10-tetraazacyclododecane-1,4,7-tricarboxylate, P2:** To a dry, 100 mL Schlenk flask equipped with a stir bar and under Argon atmosphere, CuI (7.60 mg, 0.04 mmol), TBTA (21.20 mg, 0.04 mmol) and anhydrous THF (20 mL) were added. The resulting mixture was stirred for 30 min, then tri-tert-butyl 10-(prop-2-yn-1-yl)-1,4,7,10-tetraazacyclododecane-1,4,7-tricarboxylate **3** (1.02 g, 2.0 mmol), 3-azido-N,N-bis(3-(triethoxysilyl)propyl)propan-1-amine **5** (1.02 g, 2.0 mmol) and anhydrous Et<sub>3</sub>N (1.0 mL, 0.73 g/mL 7.2 mmol) were added by using a syringe. The resulting mixture was stirred at 50 °C (Argon atmosphere) until **3** was fully consumed (48 h, TLC monitoring). Then, the solvent was evaporated under reduced pressure and hot anhydrous pentane was added to the residue to extract the bis-silylated product, this digestion with hot pentane was repeated several times and the pentane extracts were concentrated under reduced pressure to provide the pure product **P2** as colorless oil (1.80 g, 88% yield). <sup>1</sup>H NMR (360 MHz, CDCl<sub>3</sub>) δ (ppm): 7.43 (s, 1H), 4.35 (t, J = 7.2 Hz, 2H), 3.89 (s, 2H), 3.83 (q, J = 7.2 Hz, 12H), 3.35 (br s, 4H), 3.35–3.31 (m, 8H), 2.69–2.61 (m, 4H), 2.43–2.37 (m, 6H), 2.00 (t, J = 7.2 Hz, 2H), 1.50–1.43 (m, 27 + 4H), 1.21 (t, J = 7.2 Hz, 18H), 0.56 (t, J = 7.2 Hz, 4H); <sup>13</sup>C NMR (151 MHz, CDCl<sub>3</sub>) δ (ppm): 156.2, 155.7, 155.4, 141.7, 123.1, 79.5, 79.4, 79.2, 58.3, 57.2, 56.8, 54.4, 53.4, 53.1, 51.0, 50.8, 50.1, 49.7, 48.5, 48.2, 47.7, 28.7, 28.5, 28.4, 20.4, 20.2, 18.3, 8.0. IR (film): 2972.7, 2927.8, 2884.1, 2809.4, 2094.6, 1685.3, 1458.3, 1412.8, 1364.4, 1248.7, 1157.5, 1074.7, 953.8, 771.7, 702.1 cm<sup>-1</sup>. MS (ESI) m/z: 1019.7 [M + H]<sup>+</sup>, 509.3, 460.3, 410.3, 360.3; HRMS (ESI) m/z: [M + H]<sup>+</sup> calcd for C<sub>47</sub>H<sub>95</sub>N<sub>8</sub>O<sub>12</sub>Si<sub>2</sub>: 1019.6603, found: 1019.6559.

**Preparation of E-Pn 90/10 PMO NPs:** In an open 250 mL round bottom flask without reflux condenser was placed a solution of CTAB (250 mg, 0.686 mmol) in Milli-Q water (120 mL) and then 875 μL of 2 M NaOH was added (1.75 mmol of NaOH). The mixture was stirred at 1000 rpm at 80 °C for 50 min. Then, the stirring speed was enhanced to 1400 rpm and a mixture of **E** (100% E-BTSE) (704.34 mg, 2.00 mmol) with **Pn** (0.2 mmol) were added rapidly under stirring. The condensation process was conducted for two hours at 80 °C. Afterwards, the suspension was cooled to room temperature while stirring and the NPs were collected by centrifugation during 45 min at 13500 rpm. The samples were then extracted three times with a solution of NH<sub>4</sub>NO<sub>3</sub> (6 g/L in 96% EtOH), and washed three times with 96% ethanol, Milli-Q water, 96% ethanol, successively.<sup>[13]</sup> The **E-Pn 90/10 PMO NPs** were obtained as white solids. **E-P1 90/10 PMO NPs:** <sup>13</sup>C CP-MAS NMR (75 MHz) δ (ppm): 156, 142, 125, 79, 58, 51, 29, 21, 11. IR ν (ATR) (cm<sup>-1</sup>): 3334.8, 2976.5, 1673.8, 1416.7, 1187.2, 1038.5, 924.7, 790.1, 424.2. BET: S<sub>BET</sub> = 513 m<sup>2</sup>g<sup>-1</sup>, V<sub>pore</sub> = 0.29 cm<sup>3</sup>g<sup>-1</sup>, ϕ<sub>pore</sub> = 2.3 nm. TGA (air, 5 °C/min, 20–1000 °C) residual mass 60%. Zeta Potential: ζ = 39.4 mV, pH = 6.66. DLS: 520 nm. **E-P2 90/10 PMO NPs:** <sup>13</sup>C CP-MAS NMR (75 MHz) δ (ppm): 156, 146, 125, 79, 58, 49, 29, 20, 17, 11. IR ν (ATR) (cm<sup>-1</sup>): 3358.4, 2976.8, 1667.9, 1417.3, 1188.1, 1040.3, 924.6, 792.3, 423.8. BET: S<sub>BET</sub> = 492 m<sup>2</sup>g<sup>-1</sup>, V<sub>pore</sub> = 0.25 cm<sup>3</sup>g<sup>-1</sup>, ϕ<sub>pore</sub> = 2.0 nm. TGA (air, 5 °C/min, 20–1000 °C) residual mass 68%. Zeta Potential: ζ = 34.0 mV, pH = 6.25. DLS: 621 nm.

**Preparation of E-Pn 75/25 PMO NPs:** In an open 250 mL round bottom flask without reflux condenser was placed a solution of CTAB (250 mg, 0.686 mmol) in Milli-Q water (120 mL) and then 875 μL of 2 M NaOH was added (1.75 mmol of NaOH). The mixture was stirred at 1000 rpm at 80 °C for 50 min. Then, the stirring speed was enhanced to 1400 rpm and a mixture of **E** (100% E-BTSE) (581.09 mg, 1.65 mmol) with **Pn** (0.55 mmol) were added rapidly under stirring. The condensation process was conducted for two hours at 80 °C. Afterwards, the suspension was cooled to room temperature while stirring and the NPs were collected by centrifugation during 45 min at 13500 rpm. The samples were then

extracted three times with a solution of  $\text{NH}_4\text{NO}_3$  (6 g/L in 96% EtOH), and washed three times with 96% ethanol, Milli-Q water, 96% ethanol, successively.<sup>[13]</sup> The **E-Pn 75/25 PMO NPs** were obtained as white solids. **E-P1 75/25 PMO NPs**:  $^{13}\text{C}$  CP-MAS NMR (75 MHz)  $\delta$  (ppm): 156, 146, 139, 125, 80, 58, 50, 40, 29, 21, 17, 11. IR  $\nu$  (ATR) ( $\text{cm}^{-1}$ ): 3359.9, 2933.4, 1670.8, 1416.0, 1038.5, 923.9, 791.1. BET:  $S_{\text{BET}} = 162 \text{ m}^2 \text{ g}^{-1}$ ,  $V_{\text{pore}} = 0.09 \text{ cm}^3 \text{ g}^{-1}$ ,  $\phi_{\text{pore}} = 2.2 \text{ nm}$ . TGA (air,  $5^\circ\text{C}/\text{min}$ , 20–1000 $^\circ\text{C}$ ) residual mass 53%. Zeta Potential:  $\zeta = 32.7 \text{ mV}$ ,  $\text{pH} = 6.08$ . DLS: 639 nm. **E-P2 75/25 PMO NPs**:  $^{13}\text{C}$  CP-MAS NMR (75 MHz)  $\delta$  (ppm): 156, 146, 124, 79, 56, 48, 29, 19, 11. IR  $\nu$  (ATR) ( $\text{cm}^{-1}$ ): 3351.3, 2975.5, 1667.7, 1417.2, 1187.0, 1040.7, 928.1, 790.3, 424.3. TGA (air,  $5^\circ\text{C}/\text{min}$ , 20–1000 $^\circ\text{C}$ ) residual mass 55%. Zeta Potential:  $\zeta = 41.2 \text{ mV}$ ,  $\text{pH} = 4.66$ . DLS: 463 nm.

**Preparation of E-Pn' PMO NPs**: The **E-Pn PMO NPs** were dissolved in a 5:1 solution of TFA/ $\text{CH}_2\text{Cl}_2$ , the mixture was stirred at room temperature for 1–2 hour. Then the NPs were collected by centrifugation, and washed with  $\text{CH}_2\text{Cl}_2$ , saturated  $\text{NaHCO}_3$  solution (twice), water (twice), EtOH (twice), acetone. Finally, the new **E-Pn' PMO NPs** were dried under vacuum for several hours. **E-P1' 90/10 PMO NPs**:  $^{13}\text{C}$  CP-MAS NMR (75 MHz)  $\delta$  (ppm): 147, 125, 52, 46, 22, 12. IR  $\nu$  (ATR) ( $\text{cm}^{-1}$ ): 3338.4, 1187.9, 1034.7, 924.5, 790.3, 429.9. BET:  $S_{\text{BET}} = 705 \text{ m}^2 \text{ g}^{-1}$ ,  $V_{\text{pore}} = 0.43 \text{ cm}^3 \text{ g}^{-1}$ ,  $\phi_{\text{pore}} = 2.4 \text{ nm}$ . Zeta Potential:  $\zeta = 42.5 \text{ mV}$ ,  $\text{pH} = 5.30$ . EDS: 28.27% C, 32.81% O, 32.67% Si, 6.26% N. **E-P2' 90/10 PMO NPs**:  $^{13}\text{C}$  CP-MAS NMR (75 MHz)  $\delta$  (ppm): 146, 125, 58, 49, 22, 11. IR  $\nu$  (ATR) ( $\text{cm}^{-1}$ ): 3374.1, 1188.5, 1035.1, 924.1, 790.8. BET:  $S_{\text{BET}} = 645 \text{ m}^2 \text{ g}^{-1}$ ,  $V_{\text{pore}} = 0.34 \text{ cm}^3 \text{ g}^{-1}$ ,  $\phi_{\text{pore}} = 2.1 \text{ nm}$ . Zeta Potential:  $\zeta = 40.3 \text{ mV}$ ,  $\text{pH} = 5.34$ . EDS: 32.43% C, 35.09% O, 28.70% Si, 3.78% N. **E-P1' 75/25 PMO NPs**:  $^{13}\text{C}$  CP-MAS NMR (75 MHz)  $\delta$  (ppm): 146, 125, 58, 49, 22, 11. IR  $\nu$  (ATR) ( $\text{cm}^{-1}$ ): 2935.8, 1410.4, 1187.4, 1027.5, 791.7, 431.6. BET:  $S_{\text{BET}} = 202 \text{ m}^2 \text{ g}^{-1}$ ,  $V_{\text{pore}} = 0.10 \text{ cm}^3 \text{ g}^{-1}$ ,  $\phi_{\text{pore}} = 2.1 \text{ nm}$ . Zeta Potential:  $\zeta = 38.6 \text{ mV}$ ,  $\text{pH} = 5.31$ . EDS: 27.46% C, 33.58% O, 28.08% Si, 8.33% N. **E-P2' 75/25 PMO NPs**:  $^{13}\text{C}$  CP-MAS NMR (75 MHz)  $\delta$  (ppm): 146, 124, 58, 49, 23, 12. IR  $\nu$  (ATR) ( $\text{cm}^{-1}$ ): 2935.5, 1187.7, 1030.9, 931.9, 791.9, 426.7. Zeta Potential:  $\zeta = 39.6 \text{ mV}$ ,  $\text{pH} = 5.30$ . EDS: 38.15% C, 30.29% O, 23.62% Si, 7.95% N.

**Uptake of  $\text{Ni}^{2+}$  and  $\text{Co}^{2+}$  by E-P1' 90/10 PMO NPs**: 20 mg of sample and 20 mL of metal solution (10.5 mM and 9.5 mM initial metal concentration Ni and Co respectively) were introduced in a 50 mL plastic tube and put on a shaker for 70 hours. For each heavy metal triplicate experiments were performed and standard errors were measured. After set interval of times (0.5 h, 1 h, 1.5 h, 18 h, 22 h, 46 h, 70 h), **E-P1' 90/10 PMO NPs** were centrifuged (7000 g) for 10 min and 1 mL aliquot was separated to determine the metal concentration in the remaining solution. The sample was first diluted 5 times, and titrated afterwards with EDTA and xylenol orange as an indicator. For each sample the titrations were repeated 3 times, and the average was calculated. The uptake was calculated according to this equation:  $U_p = (\text{Co} - \text{Ce}) * V/m$ . Where: Co is the initial metal concentration which was also measured by titration, Ce is the equilibrium concentration of the metals after set interval of times, V is the volume of initial metal solution which was kept constant, m is the NPs weight.

**Desorption tests for E-Pn' PMO NPs**: The samples **E-P1' 75/25** and **E-P2' 90/10 PMO NPs** were performed with 1 M nitric acid in 50 mL tubes. After adsorption experiments the samples were centrifuged and 20 mL nitric acid was then added. The tubes were placed on a shaker for 24 hours. Then nanoparticles were centrifuged and the solution was neutralized with ammonium hydroxide and titrated with EDTA to calculate the desorbed metal amount. The nanoparticles were dried and the remaining metal content was measured with EDS (the metal uptake was measured with EDS also before desorption test).

**Selectivity experiment with mixed metal solution**: For this procedure around 10 mg of recycled nanoparticles (**E-P2' 75/25 PMO NPs**) were mixed with equimolar mixture of Nd–Ni and Co–Sm (5 mM initial concentration each) for 24 hours. Afterwards, nanoparticles were separated and dried and the metal content was analyzed by EDS spectroscopy.

## Supporting Information

Supporting Information is available from the Wiley Online Library or from the author.

## Acknowledgements

This research was funded by China Scholarship Council (CSC) (H.L., No. 201606890025), Ministerio de Ciencia, Innovación y Universidades (MCIU) of Spain (Project RTI2018-097853-B-I00 and RED2018-102387-T), DURSI-Generalitat de Catalunya (Project SGR2017-0465) and ERA-MIN 2 MetRecycle project supported in Sweden by Vinnova grant No. 2018-00739. The authors are grateful to Dr. Míriam Pérez-Trujillo (NMR Service of UAB) who helped us interpret the NMR spectra. Hitach High-Tech Sweden AB is gratefully acknowledged for the loan of Flex-SEM 1000 II instrument and user guidance.

## Conflict of Interest

The authors declare no conflict of interest.

**Keywords:** periodic mesoporous organosilica nanoparticles · structural characterization · cyclen functionalization · metal adsorption · REE separation from heavy metals

- [1] a) R. S. Guimarães, C. F. Rodrigues, A. F. Moreira, I. J. Correia, *Pharmacol. Res.* **2020**, *155*, 104742; b) Z. Teng, W. Li, Y. Tang, A. Elzatahy, G. Lu, D. Zhao, *Adv. Mater.* **2018**, *0*, 1707612; c) J. G. Croissant, Y. Fatieiev, A. Almalik, N. M. Khashab, *Adv. Healthcare Mater.* **2018**, *7*, 1700831; d) X. Du, X. Li, L. Xiong, X. Zhang, F. Kleitz, S. Z. Qiao, *Biomaterials* **2016**, *91*, 90–127; e) Y. Chen, J. Shi, *Adv. Mater.* **2016**, *28*, 3235–3272; f) J. G. Croissant, X. Cattoen, M. Wong Chi Man, J.-O. Durand, N. M. Khashab, *Nanoscale* **2015**, *7*, 20318–20334.
- [2] M. Jahns, D. P. Warwas, M. R. Krey, K. Nolte, S. König, M. Fröba, P. Behrens, *J. Mater. Chem. B* **2020**, *8*, 776–786.
- [3] L. Wang, C. Cheng, S. Tapas, J. Lei, M. Matsuoka, J. Zhang, F. Zhang, *J. Mater. Chem. A* **2015**, *3*, 13357–13364.
- [4] a) M. A. O. Lourenço, P. Figueira, E. Pereira, J. R. B. Gomes, C. B. Lopes, P. Ferreira, *Chem. Eng.* **2017**, *322*, 263–274; b) P. Figueira, M. A. O. Lourenço, E. Pereira, J. R. B. Gomes, P. Ferreira, C. B. Lopes, *J. Environ. Chem. Eng.* **2017**, *5*, 5043–5053.
- [5] a) V. V. Sliesarenko, O. A. Dudarko, Y. L. Zub, G. A. Seisenbaeva, V. G. Kessler, P. Topka, O. Solcova, *J. Porous Mater.* **2013**, *20*, 1315–1321; b) I. V. Melnyk, G. I. Nazarchuk, M. Václavíková, Y. L. Zub, *Appl. Nanosci.* **2019**, *9*, 683–694; c) O. Dudarko, Y. Zub, *Chem. J. Mold.* **2017**, *12*, 79–86.
- [6] a) A. Kayan, *Adv. Compos. Hybrid Mater.* **2019**, *2*, 34–45; b) B. Samiey, C. H. Cheng, J. Wu, *Materials* **2014**, *7*, 673–726.
- [7] S. Yang, S. Chen, J. Fan, T. Shang, D. Huang, G. Li, *J. Colloid Interface Sci.* **2019**, *554*, 565–571.
- [8] A. M. Kaczmarek, S. Abednatanzi, D. Esquivel, C. Krishnaraj, H. S. Jena, G. Wang, K. Leus, R. Van Deun, F. J. Romero-Salguero, P. Van Der Voort, *Microporous Mesoporous Mater.* **2020**, *291*, 109687.

- [9] L. Su, J. Ma, J. Wang, W. Jiang, W.X. Zhang, J. Yang, *Chem. Commun.* **2020**, *56*, 2795–2798.
- [10] a) P. Lejault, K. Duskova, C. Bernhard, I.E. Valverde, A. Romieu, D. Monchaud, *Eur. J. Org. Chem.* **2019**, *2019*, 36 6146–6157; b) D. Mukherjee, J. Okuda, *Chem. Commun.* **2018**, *54*, 2701–2714.
- [11] a) K. Jobe, C. H. Brennan, M. Motevalli, S. M. Goldup, M. Watkinson, *Chem. Commun.* **2011**, *47*, 6036–6038; b) S. Hwang, W. Cha, M. E. Meyerhoff, *Angew. Chem. Int. Ed.* **2006**, *45*, 2745–2748; *Angew. Chem.* **2006**, *118*, 2811–2814.
- [12] K. Bürglová, N. Moitra, J. Hodacová, X. Cattoën, M. Wong Chi Man, *J. Org. Chem.* **2011**, *76*, 7326–7333.
- [13] a) H. Li, L. Raehm, C. Charnay, J.-O. Durand, R. Pleixats, *Materials* **2020**, *13*, 1569; b) H. Li, C. Gasco, A. Delalande, C. Charnay, L. Raehm, P. Midoux, C. Pichon, R. Pleixats, J.-O. Durand, *Molecules* **2020**, *25*, 974.
- [14] V. V. Tomina, I. V. Melnyk, Y. L. Zub, A. Kareiva, M. Vaclavikova, G. A. Seisenbaeva, V. G. Kessler, *Beilstein J. Nanotechnol.* **2017**, *8*, 334–347.
- [15] E. Polido Legaria, M. Samouhos, V. G. Kessler, G. A. Seisenbaeva, *Inorg. Chem.* **2017**, *56*, 13938–13948.

---

Manuscript received: July 1, 2020

Revised manuscript received: September 2, 2020

Accepted manuscript online: September 15, 2020

Version of record online: September 24, 2020

---